Highway Modeling. Part II: Advection and Diffusion of SF_6 Tracer Gas

ROBERT E. ESKRIDGE[1] AND FRANCIS S. BINKOWSKI[1]

Environmental Sciences Research Laboratory, Environmental Protection Agency, Research Triangle Park, NC 27711

J. C. R. HUNT[2]

Department of Applied Mathematics and Theoretical Physics, University of Cambridge, Cambridge, England EB3 9EW

TERRY L. CLARK[1] AND KENNETH L. DEMERJIAN[1]

Environmental Sciences Research Laboratory, Environmental Protection Agency, Research Triangle Park, NC 27711

(Manuscript received 3 July 1978, in final form 4 December 1978)

ABSTRACT

A finite-difference highway model is presented which uses surface layer similarity theory and a vehicle wake theory to determine the atmospheric structure along a roadway. Surface similarity is used to determine the wind profile and eddy diffusion profiles in the ambient atmosphere. The ambient atmosphere is treated as a basic-state atmosphere on which the disturbances due to vehicle wakes are added. A conservation of species equation is then solved using an upstream-flux corrected technique which insures positive concentrations. Simulation results from the highway model are compared with 58 half-hour periods of data (meteorological and SF_6 tracer) taken by General Motors. The results show that the predictions of this model are closer to the observations than those of the Gaussian-formulated EPA highway model (HIWAY).

1. Introduction

In Part I of this series of papers (Eskridge and Hunt, 1979) a theory was developed for the velocity and turbulence field behind a single vehicle and applied to the multi-vehicle case of the General Motors experiment (Cadle *et al.*, 1976). This paper describes a model which uses wake theory and surface-layer similarity theory to predict pollutant concentrations along a roadway.

The wake and similarity theories are used together to predict the wind field and eddy diffusion coefficient fields along the roadway. This is in contrast to other roadway models which have not completely addressed the problem of determining K_x and K_z (Egan *et al.*, 1973; Kirsch and Mason, 1974) or approaches such as that of Danard (1972) who specified K as 20 m^2 s^{-1} on the roadway which is much too large. Ragland and Peirce (1973) did use a similarity theory approach for the ambient conditions but did not include vehicular effects on the wind or turbulence fields.

In this paper a review of the GM sulfate-dispersion experiment and data is presented in Section 2. The model, boundary conditions and numerical scheme are given in Section 3, while in Section 4 the similarity theory and technique for calculating the eddy diffusion coefficients in the basic state or ambient atmosphere is presented. In Section 5 a summary of the pertinent wake theory results is given together with the methods used for obtaining eddy diffusion coefficients along the highway. The results for two 30 min simulations are presented in Section 6 together with scatter diagrams for all experiments and other analyses of the predictions.

2. The General Motors sulfate-dispersion experiment

The GM experiment was held in September and October of 1975 at the GM proving grounds in Milford, Michigan. A fleet of 352 automobiles were driven on a north–south track of 10 km length for 17 days during the morning hours. [See Cadle *et al.* (1976), for a complete description of the experiment and analysis procedure.]

Meteorological instruments and chemical samplers were located on six towers and two stands 2.4 km north of the south end of the test track (see Figs. 1

[1] On assignment to EPA from NOAA.

[2] Work done while a visiting professor at North Carolina State University, Raleigh, supported by EPA Grant R80 4653.

0021-8952/79/040401-12$07.00

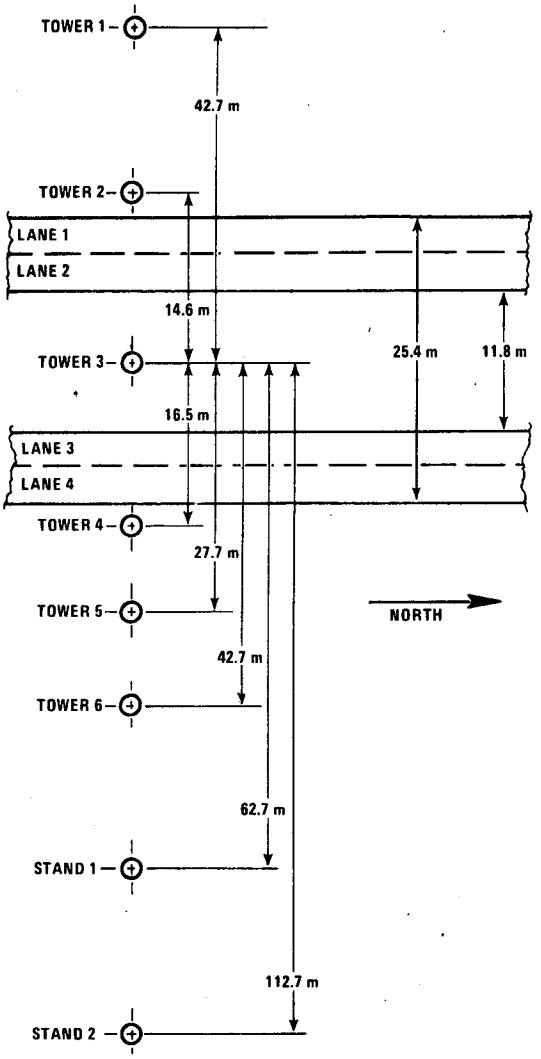

FIG. 1. Orientation of test track and perpendicular distances of the meteorological towers from the center of the test track.

and 2). Wind speeds from the 20 Gill UVW anemometers were recorded once per second. The wind instruments were located on the towers approximately 1.5, 4.4 and 10.44 m above the surface and the syringe samplers used to sample SF_6 were located at 0.5, 3.5 and 9.5 m above the surface. Temperature data were recorded from towers 1 and 6 every 5 s using a Rosemount Model 78-0039-0023 single-element, platinum-resistance thermometers mounted in Model 43404 Gill aspirated temperature shields. The temperature instruments were located approximately at the same heights as the UVW instruments.

Packs of 22 cars were spaced 300 m apart with the lead car traveling 80 km h^{-1}. Uniformly distributed through the 16 packs were seven or eight pickup trucks that released SF_6 tracer gas. Sampling began approximately 5 min after the vehicles started around the track. Four sequential samples, each taken over a 30 min period, were analyzed for SF_6 at each observation point. Sampling of SF_6 was accomplished using a modified Developmental Science syringe sampler which collected a 30 cm^3 sample in a 30 min period. The samples were analyzed using an automatic dual-column gas chromatograph equipped with electron capture detectors. Analysis accuracy was estimated to be within $\pm 6\%$. Problems occurred on two of the days with the release of SF_6; therefore, the total number of sample periods is 58 instead of 66.

3. The model

Since there seldom exists sufficient information on the wind field to do a three-dimensional analysis or prediction of the wind field along a roadway, it is assumed that the derivative parallel to the road is zero $(\partial/\partial y=0)$. The model domain is therefore in the x-z plane (see Fig. 3). It is assumed that the terrain is flat and homogeneous.

a. The equation

The general form of a conservation of species equation, neglecting chemical reactions, is

$$\frac{\partial A}{\partial t}+\nabla_2\cdot AV=\nabla_2\cdot K\nabla_2 A+E(\mathbf{x},t), \qquad (1)$$

where ∇_2 is the divergence operator in x and z coordinates, $E(\mathbf{x},t)$ an emission source term, K the eddy diffusion coefficient and A some chemical species. In

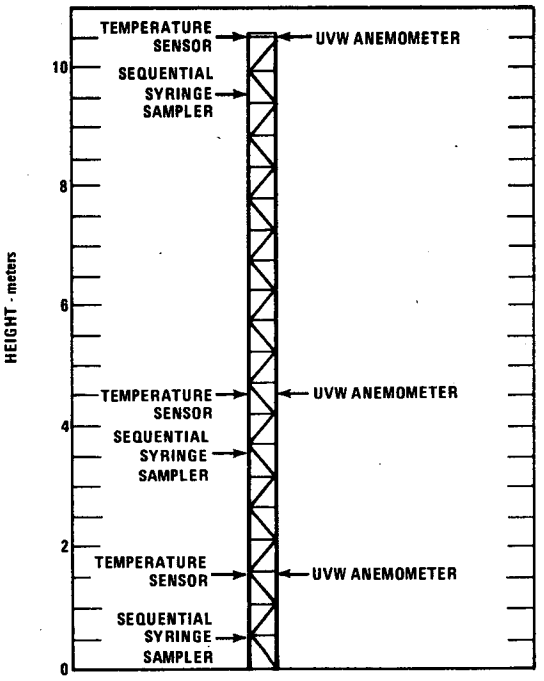

FIG. 2. Approximate height of instruments above the ground for the six towers.

the case of the GM experiment A will represent SF_6.

One of the main assumptions made is that a reference atmosphere describable by similarity theory exists on which the perturbations due to the vehicles can be added, i.e.,

$$\left.\begin{aligned} K_x &= K_x^s(z)+K_x^w(x,z) \\ K_z &= K_z^s(z)+K_z^w(x,z) \end{aligned}\right\}, \tag{2}$$

where K_x^s and K_x^w are the eddy diffusion coefficients from similarity and wake theories, respectively. Similarly, the wake velocity deficit is added to the wind field predicted by similarity.

Physical reasoning and numerical stability require that $\nabla_2 \cdot \mathbf{V}=0$, hence the continuity equation is solved to yield W, the vertical velocity, which is not zero along the road due to the presence of the vehicle wakes.

b. The boundary conditions

The problem of imposing boundary conditions is always difficult in atmospheric modeling especially when the scale of the problem is small. In this model it is assumed that the gradient at the surface is zero, i.e.,

$$\frac{\partial A}{\partial z}=0 \quad \text{at} \quad z=0, \tag{3}$$

which implies no losses at that boundary. At the side boundaries, the zero gradient condition

$$\frac{\partial A}{\partial x}=0 \quad \text{at} \quad x=0, x_{\max} \tag{4}$$

is imposed. At the top it is assumed that the concentration is zero, i.e.,

$$A=0 \quad \text{at} \quad z=z_{\max}. \tag{5}$$

These boundary conditions [Eqs. (4) and (5)] are not perfect physical constraints as they are imposed only for mathematical reasons. It has been found in experimentation that the model results were more sensitive to the height of the modeling region than to any boundary condition. Therefore, when the winds are light or parallel to the roadway, the height of the integration region is raised from 30 to 90 m.

c. The grid

The numerical solution of (1) requires that it be expressed in finite differences on some grid. The grid lengths are chosen such that in the x direction, Δx is equal to the width of one traffic land and $\Delta z/2$ is approximately the height of an automobile (see Fig. 3).

d. The numerical scheme

Eq. (1) can be written in operator form as

$$\frac{\partial A}{\partial t}+B_1A+B_2A+B_3A+B_4A=E, \tag{6}$$

where B_1, B_2, B_3 and B_4 are linear operators, and represent $\partial u(\ )/\partial x$, $\partial w(\ )/\partial x$, $-(\partial/\partial x)K_x\partial(\ )/\partial x$ and $-(\partial/\partial z)K_z\partial(\ )/\partial z$, respectively. Eq. (6) can be approximated by

$$\frac{A^{n+1}-A^n}{\Delta t}+\sum_{m=1}^{4}\Lambda_m A_{ik}=E_{ik}, \tag{7}$$

where Λ_m, $m=1,\ldots,4$ are approximations of B_m $(x=i\Delta x,\ z=k\Delta z-0.5z,\ t=n\Delta t)$. Eq. (7) will be solved by a fractional step method (Marchuk, 1975). The procedure is as follows:

$$A^1 = A^n+\Delta t\Lambda_1 A^n \tag{8}$$

$$A^2 = A^1+\Delta t\Lambda_2 A^1 \tag{9}$$

$$A^3 = A^2+\Delta t\Lambda_3 A^2 \tag{10}$$

$$A^4 = A^3+\Delta t\Lambda_4 A^3 \tag{11}$$

$$A^{n+1}=A^4+\Delta t E_{ik}. \tag{12}$$

If one eliminates $A^1,\ldots,A^4$, the system reduces to an

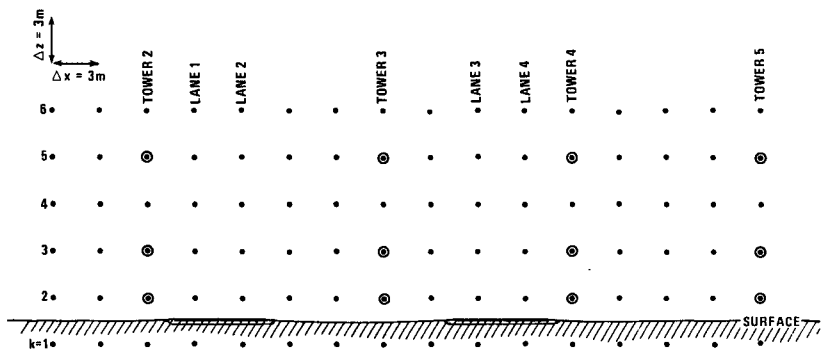

FIG. 3. Schematic representation of part of the difference net showing highway lane locations and the location of towers 2, 3, 4 and 5 in terms of the finite-difference net. The circles around net points denote approximate UVW anemometer locations.

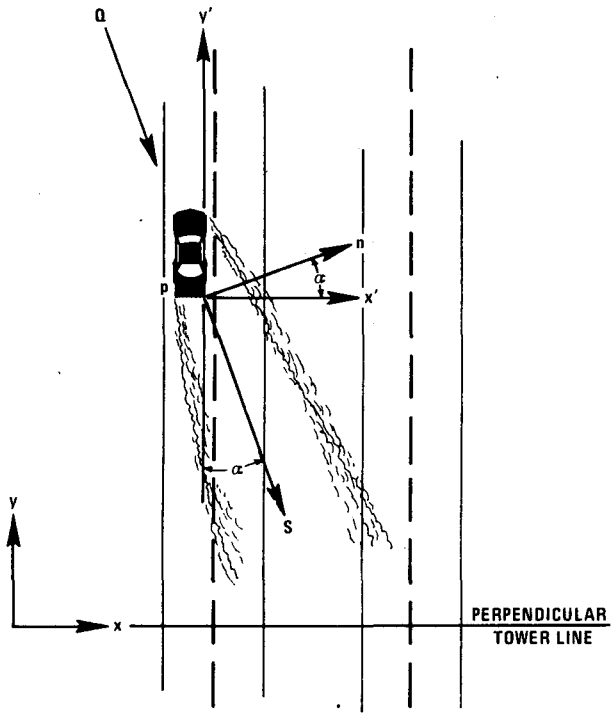

FIG. 4. The s,n,z coordinate system, oriented along the wake and normal to it, and the x,y,z system, fixed in a east–west, north–south orientation.

equation of the form

$$A^{n+1}=A^n+\Delta t\sum_m \Lambda_m A^n+\Delta t E_{ik}+(\Delta t)^2(\cdots)$$
$$+\text{higher order terms.} \quad (13)$$

The operators Λ_3, Λ_4 are simply centered in space approximations, while the operators Λ_1, Λ_2, which solve

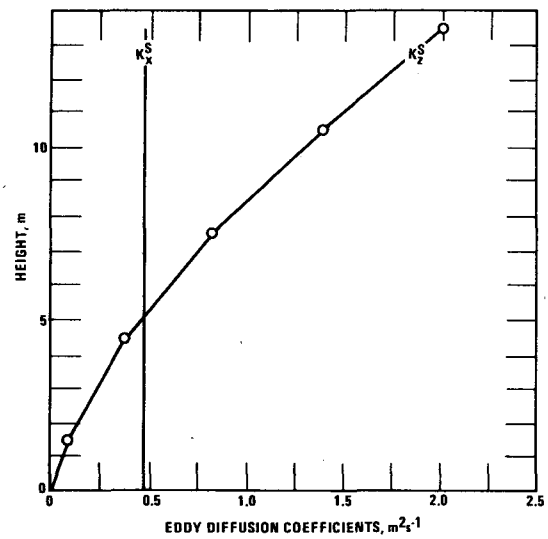

FIG. 5. Eddy diffusion coefficients predicted by similarity theory for ambient atmosphere for case 2830920.

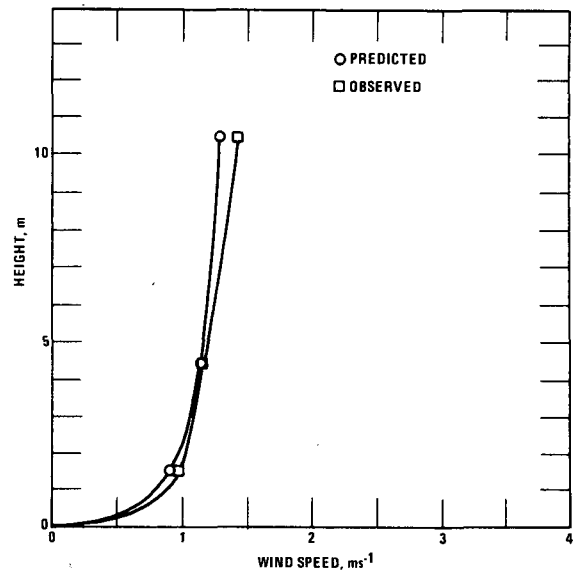

FIG. 6. Observed and similarity predicted wind profile for ambient atmosphere for case 2830920.

the flux terms, are based on a flux-corrected algorithm of Zalesak (1976, private communication). This algorithm is an upstream scheme which insures non-negative values for the concentration at every grid point. (Details of this technique are given in the Appendix.)

The assurance of positive values is important since Eskridge and Demerjian (1977) have shown that negative concentrations combined with nonlinear chemistry can result in unstable numerical schemes. The algorithm also reduces numerical diffusion and is stable for

$$\Delta t \leqslant \frac{0.5\Delta x}{u_{\max}}. \quad (14)$$

Because of the complexity of this algorithm it has not been possible to show that the fractional step method is compatible with the original differential equation. However, if an upstream approximation is used to calculate the flux terms it can be shown that the truncation error (the difference between the partial differential equation and the approximation) for the fractional step method is

$$O(\Delta t)+O(\Delta x)+O(\Delta t/\Delta x). \quad (15)$$

The complexity of the flux algorithm also prevents establishing the fact that the procedure is stable. Experience has shown that, if every separate step is stable, the calculation is stable.

The upstream algorithm, while not as accurate as a centered scheme, such as SHASTA (Boris and Book, 1973), has the advantage of requiring only one point outside the integration region for boundary conditions.

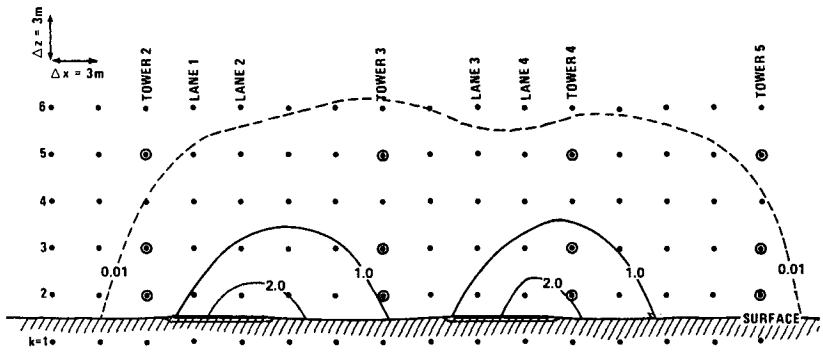

FIG. 7. Predicted K_x^w field from wake theory for 2830920.

4. The basic-state atmosphere

The wind profiles used in the model are obtained from similarity theory [see Busch (1973) for a review] in the following manner. Since the Obukhov length L is very difficult to measure directly, the bulk Richardson number is used as a stability parameter

$$R_b=\frac{gh\Delta\theta}{\theta_h U_h^2}, \tag{16}$$

when g is the acceleration due to gravity, h the height of the wind observation, U_h the wind speed at height h, θ_h the potential temperature at h and $\Delta\theta$ the difference in potential temperature between two tower points. The temperature difference is taken over the height increment $(h-z_1)$, where the height z_1 of the lower instrument is assumed to be small enough relative to h so that $\Delta\theta$ is representative of a temperature difference over the entire distance h. The Obukhov length L may be expressed as (Nickerson and Smiley, 1975; Benoit, 1977)

$$L=\frac{hG(h)}{kF^2(h)R_b}, \tag{17}$$

where

$$F(h)=\frac{1}{k}\left[\ln\left(\frac{h}{z_0}\right)+P\left(\frac{h}{L}\right)\right], \tag{18}$$

$$G(h)=\frac{1}{k}\left[\ln\left(\frac{h}{z_1}\right)+Q\left(\frac{h}{L}\right)\right], \tag{19}$$

$$P(h/L)=\ln\{[(X_0^2+1)(X_0+1)^2/[(X^2+1)(X+1)^2]\}+2[\tan^{-1}X-\tan^{-1}X_0], \tag{20}$$

where

$$X=(1-16h/L)^{\frac{1}{4}},\quad X_0=(1-16z_0/L)^{\frac{1}{4}} \tag{21}$$

for $L<0$ (unstable)

$$P(h/L)=5(h-z_0)/L \quad \text{for} \quad L>0 \text{ (stable)}, \tag{22}$$

$$Q(h/L)=2\ln[(Y_1+1)/(Y+1)], \tag{23}$$

$Y=X^2$, $Y_1=(1-16z_1/L)^{\frac{1}{2}}$ for $L<0$ (unstable,

$$Q(h/L)=5(h-z_1)/L \quad \text{for} \quad L>0 \text{ (stable)}. \tag{24}$$

The values of X, X_0, Y and Y_1 are taken from the profiles of Dyer (1974), and Eqs. (18)–(24) are quadratures of these profiles over z/L.

Given a value of R_b, Eq. (17) is solved by an iterative process to return a value of L. The present method has an error in reproducting a given L of at most 0.08% in the range $-4\leqslant z/L\leqslant 4$. The number of iterations can be increased to improve the accuracy since only three iterations are used in the unstable case and five iterations in the stable case. In the following discussion of the similarity theory [Eqs. (25)–(42)], the wind speed u is oriented along the

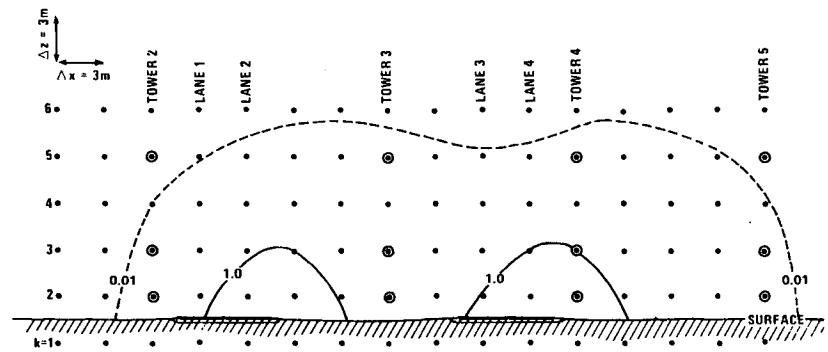

FIG. 8. As in Fig. 7 except K_z^w field.

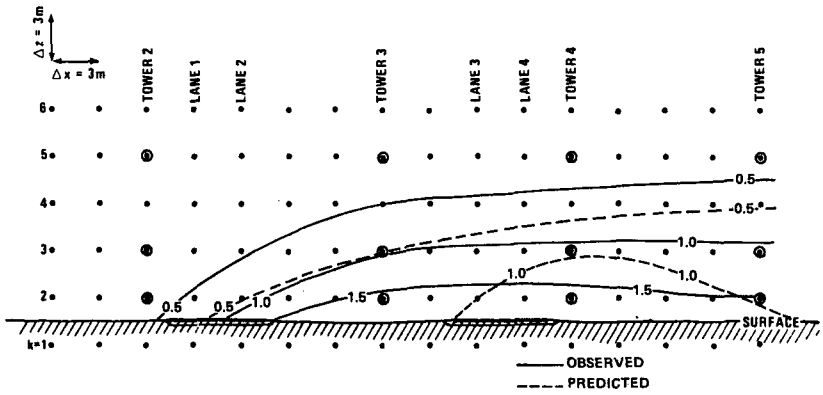

FIG. 9. Contours of half-hour averaged SF_6 concentrations.

direction of the wind, whereas in the rest of this paper u is the component of the wind along the x axis.

The friction velocity u_*, the scaling temperature T_* and the extrapolated temperature T_0 at z_0 are then obtained as follows:

$$u_* = U_h/F(h), \tag{25}$$

$$T_* = \Delta\theta/G(h), \tag{26}$$

$$T_0 = \theta_h - \Delta\theta - T_* G_0, \tag{27}$$

where

$$G_0 = \frac{1}{k}[\ln(z_1/z_0) + Q(z_1/L)], \tag{28}$$

$$Q\left(\frac{z_1}{L}\right) = 2\ln[(Y_0+1)/(Y_1+1)],$$

$$Y_0 = X_0^{\frac{1}{2}} \quad \text{for} \quad L<0, \tag{29}$$

$$Q\left(\frac{z_1}{L}\right) = 5(z_1 - z_0)/L \quad \text{for} \quad L > 0. \tag{30}$$

Once u_*, T_* and T_0 are obtained, the profiles of u and T are available from

$$u = u_* F(z), \tag{31}$$

$$T = T_0 + T_* G(z), \tag{32}$$

where z replaces h, and z_0 replaces z_1 everywhere in Eqs. (18)–(24).

Following a suggestion of Hanna (1968) the eddy diffusivity for vertical turbulent transfer of a passive scalar is written

$$K_z = c_1 \sigma_w \lambda, \tag{33}$$

where λ is a length scale and c_1 a constant determined as follows. For steady, neutral flow in the surface layer,

$$K_z = kzu_*. \tag{34}$$

It follows from (33) and (34) that

$$c_1 = \frac{kzu_*}{\sigma_w \lambda}. \tag{35}$$

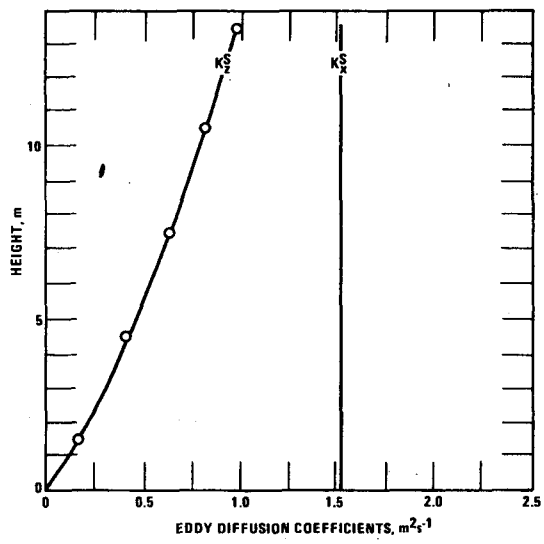

FIG. 10. As in Fig. 5 except for case 2960834.

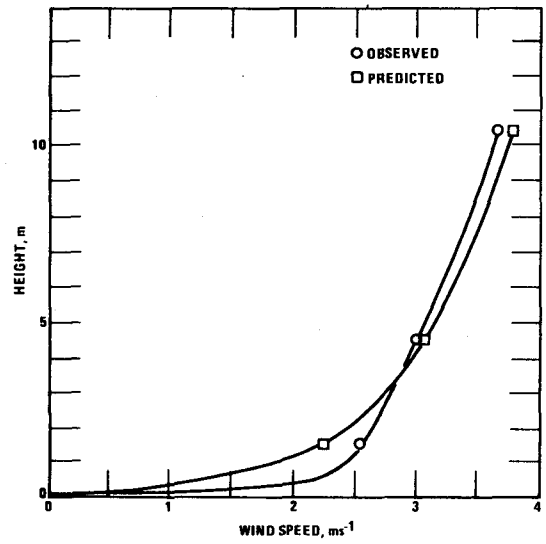

FIG. 11. As in Fig. 6 except for case 2960834.

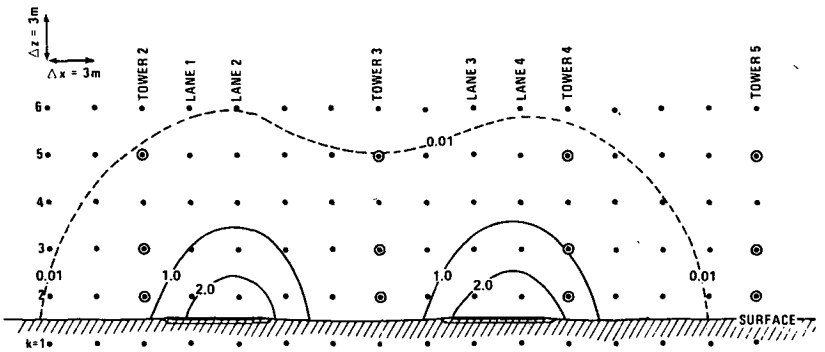

FIG. 12. As in Fig. 7 except for case 2960834.

Binkowski (1979) has shown that under neutral conditions

$$\sigma_w/u_* = 1.28, \quad z\lambda^{-1} = 0.4,$$

hence $c_1 = 0.125$. For simplicity, this neutral value will be used in all the following calculations. This method requires evaluation of σ_w and λ given R_b.

Binkowski (1979) has shown that for the surface layer

$$\frac{\sigma_w}{u_*} = \left(\frac{\phi_m - z/L}{3kf_m}\right)^{\frac{1}{3}}, \tag{36}$$

where $\phi_m = (1-16z/L)^{-\frac{1}{4}}$ for unstable cases, and $\phi_m = 1+5z/L$ for stable cases. The length scale λ in the surface layer is obtained from

$$\lambda = zf_m^{-1}, \tag{37}$$

where f_m, the nondimensional frequency at which the maximum power occurs in the w spectrum, is given by the empirical expression

$$f_m = \begin{cases} 0.4[0.4+0.6\exp(4z/L)], & z/L<0 \\ 0.4[1.0+3.39z/L-0.25(z/L)^2], & 0\leqslant z/L\leqslant 2.0 \\ 0.04[6.78+2.39(z/L-2.0)], & z/L>2 \end{cases} \tag{38}$$

which is based on the results of Kaimal (1973). Recent data presented by Wamser and Müller (1977) confirm the expressions in (38).

With the GM meteorological data, the winds and temperature from the upwind tower were used to calculate R_b assuming, for simplicity, that the anemometer and thermometer are both at the same height (4.24 or 4.4 m). This anemometer height defines h in (16) and L, u_*, T_* and T_0 from Eqs. (17) and (25)–(27). The profiles are then obtained using (31) and (32).

Estimating K_x^s [see Eq. (2)] is much more difficult and is important only when the winds have a large component parallel to the roadway. It is assumed in this model that

$$K_x^s = \begin{cases} |\sigma_u\cos\theta+\sigma_v\sin\theta|_{z=0.5\Delta z}\lambda, & z/L\geqslant 0 \\ |\sigma_u\cos\theta+\sigma_v\sin\theta|_{z=0.5\Delta z}\lambda, & z/L<0 \end{cases} \tag{39}$$

where θ is the wind direction and where σ_u and σ_v are given by

$$\frac{\sigma_u}{u_*} = \left(\frac{2.0\phi_m+R_1}{R_2}\right)^{\frac{1}{2}}, \quad \frac{\sigma_v}{u_*} = \left(\frac{R_1}{R_2}\right)^{\frac{1}{2}}, \tag{40}$$

where

$$R_1 = (3.2f_m+1.2)(\sigma_w/u_*)^3+1.4z/L, \tag{41}$$

$$R_2 = 3.2f_m\sigma_w/u_*. \tag{42}$$

The above formulation does not include the cross correlation terms. However, since the horizontal dif-

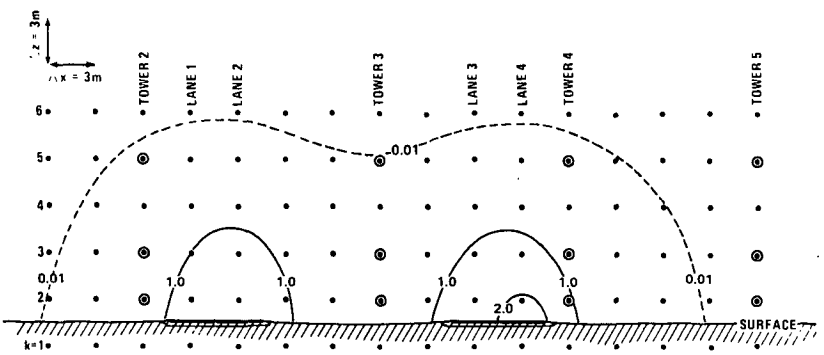

FIG. 13. As in Fig. 8 except for case 2960834.

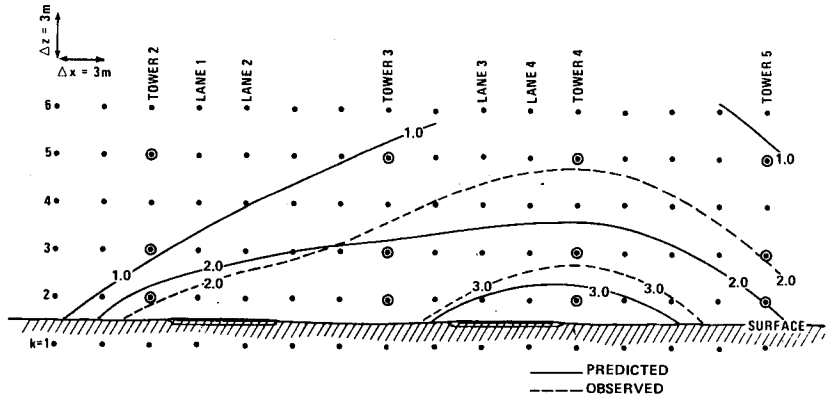

FIG. 14. As in Fig. 9 except for case 2960834.

fusion term is important only when the winds are almost parallel to the road, for this case the omission of the cross-correlation terms is of little consequence.

5. Vehicle wake theory and eddy diffusion coefficients

a. Wake theory

In Eskridge and Hunt (1979) a theory for the velocity deficit in the wake of a moving vehicle was derived from a perturbation analysis of the equations of motion.

The velocity field along the roadway for the multi-vehicle case was found to be

$$\tilde{u}(x,z)=\bar{U}_\infty(z)-\frac{1}{\Delta y}\sum_{j=1}^{N}\int_{y_j-\Delta y/2}^{y_j+\Delta y/2}\tilde{u}_s(s_j,n_j,z:x_j,y_j)\times\sin\alpha_j dy, \quad (43)$$

where $[(x_j,y_j):\delta=1,\ldots,N]$ is the distribution of the vehicles; Δy the average spacing between the vehicles; $\bar{U}_\infty$ the basic-state wind velocity; $\tilde{u}_s$ the velocity deficit in the s,n,z coordinate system (see Fig. 4); $\tilde{u}$ the x component of the wind across the road; and α_j the angle between the road and the s axis.

The turbulent fluctuations were found to be given by

$$\overline{u'^2}=\frac{1}{\Delta y}\sum_{j=1}^{N}\int_{y_j-\Delta y/2}^{y_j+\Delta y/2}(\overline{u_s'^2}\sin\alpha_j+\overline{u_n'^2}\cos\alpha_j)dy \quad (44)$$

$$\overline{w'^2}=\frac{1}{\Delta y}\sum_{j=1}^{N}\int_{y_j-\Delta y/2}^{y_j-\Delta y/2}\overline{w'^2}dy. \quad (45)$$

b. Diffusion

The diffusion along the wake of pollutant from a source on or near the vehicle producing the wake is similar to the diffusion of heat or mass in the wake of other kinds of bluff obstacles (Hinze, 1975). The diffusion can be modeled by a diffusivity because the pollutant is released near the ground and because of the self-preserving nature of the flow. Thus for a single vehicle in a moving frame of reference,

$$\left.\begin{aligned}K_x^w&\approx(\overline{u'^2})^{\frac{1}{2}}l(s)\\K_z^w&\approx(\overline{w'^2})^{\frac{1}{2}}l(s)\end{aligned}\right\}, \quad (46)$$

where $l(s)$ is the wake thickness given by $l=\gamma A[s/h]^{\frac{1}{3}}$ where γ, A and h are constants defined in Part I of this series. The advantage of this estimate is that it allows K_x and K_z to decrease across the wake, a feature not possible using an estimate based on the eddy viscosity which was assumed to be constant in the wake. It follows that in a multi-vehicle situation, K_x^w and K_z^w are given by

$$K_x^w=\frac{a_1}{\Delta y}\sum_{j=1}^{N}\int_{y_j-\Delta y/2}^{y_j+\Delta y/2}\overline{u'^2}(s_j,n_j,z:x_j,y_j)^{\frac{1}{2}}l(s_j,n_j)dy, \quad (47)$$

$$K_z^w=\frac{a_3}{\Delta y}\sum_{j=1}^{N}\int_{y_j-\Delta y/2}^{y_j+\Delta y/2}\overline{w'^2}^{\frac{1}{2}}l(s_j,n_j)dy, \quad (48)$$

where d_1 and d_3 are constants.

6. Results

In this section the results of two half-hour simulations are presented in detail together with an analysis of the results of 58 half-hour simulations. It will be shown that even though the model overpredicts pollutant concentrations, the overprediction is less than that of the EPA highway model.

Figs. 5–9 and 10–14 present the results of 30 min periods 2830920 and 2960834, respectively. [The first three digits are the Julian date, and the last four are the ending time (CST) of the data gathering period.]

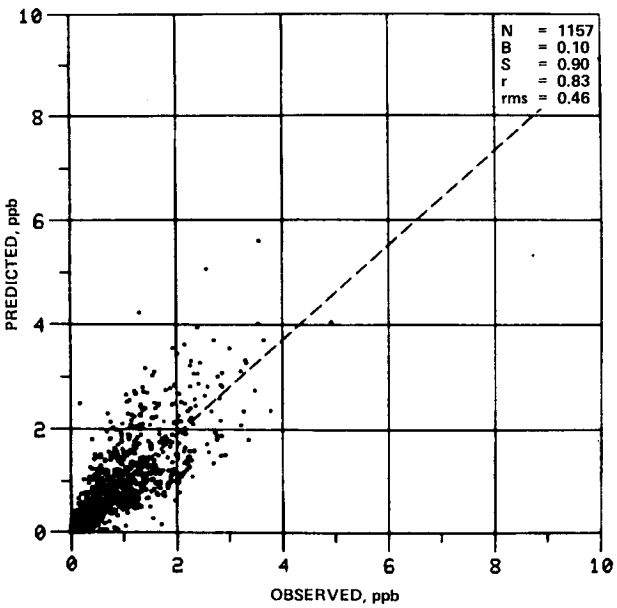

FIG. 15. Plot of observed vs predicted SF_6. The straight line is a least-squares linear fit with slope S and intercept B on the y axis; r is the correlation, N the number of data points and rms is the root-mean-square error.

From the wind and temperature data it was found that for case 2830920, $u_*=0.20$ m s^{-1}, $R_b=-3.0\times10^{-3}$ and $L=79.0$ m. The eddy diffusion coefficients for the basic atmosphere, as calculated from similarity theory, are given in Fig. 5. Fig. 6 shows the upwind observed wind profile and the predicted wind profile (the wind speed at 4.5 m was used as input).

The computed eddy-diffusion coefficients from the wake theory are presented in Figs. 7 and 8. It should be noted that the wind at 1.5 m had components of

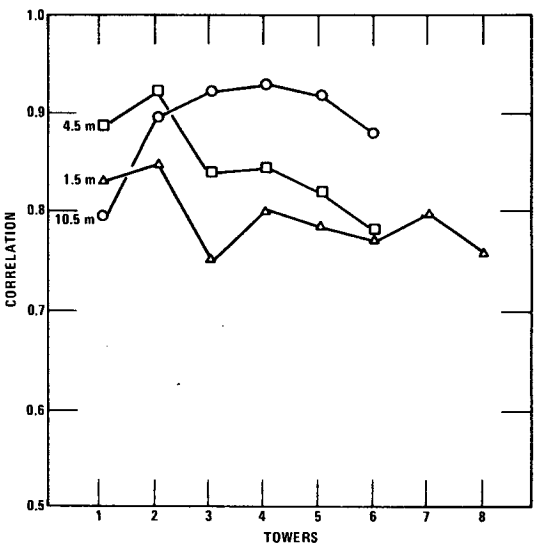

FIG. 16. Plot of the correlation between observed and predicted SF_6 for each observation point for all experiments.

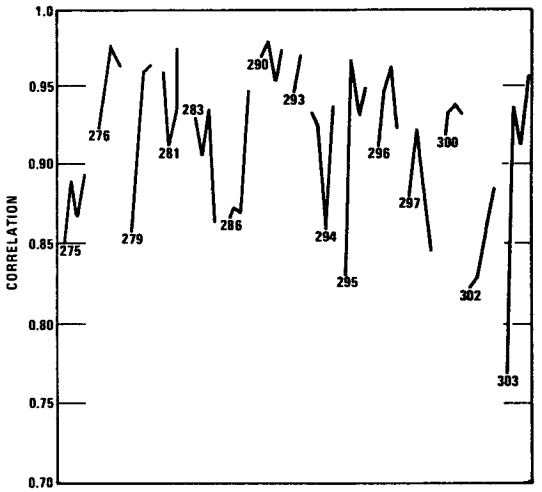

FIG. 17. Plot of the correlation between observation and prediction for the 20 sampling locations for each half-hour period. The numbers in the graph are the Julian date of the experiments.

$u=0.78$ m s^{-1} and $v=0.45$ m s^{-1} and that this, as expected, results in the eddy diffusion fields being advected downwind and having larger values in lanes 3 and 4.

Fig. 9 shows an analysis of the observed and predicted SF_6 concentration fields near the roadway. The predicted concentrations are considerably less than the observed which may imply that the wake theory is predicting K_x and K_z values that are too large. This arises because several constants used in the wake theory in determining the magnitude of the turbulence in the wake (in Part I these constants are a_1,a_2,a_3) have not been determined by physical experiments, but by computer experiments, and are subject to an uncertainty in the actual values.

Case 2960834 is for winds almost parallel to the

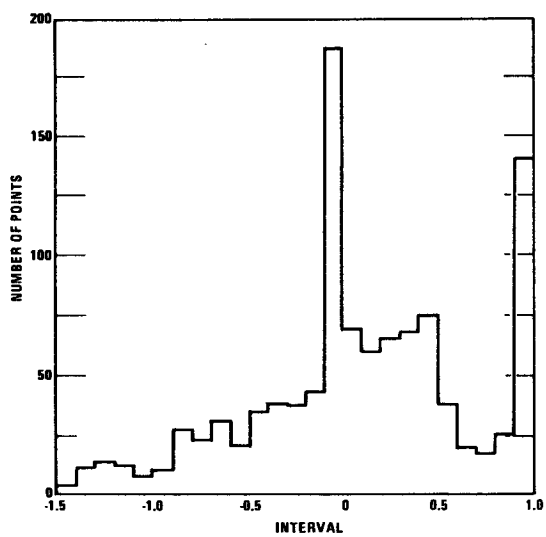

FIG. 18. Plot of frequency distribution of (O−P)/O for intervals of 0.1.

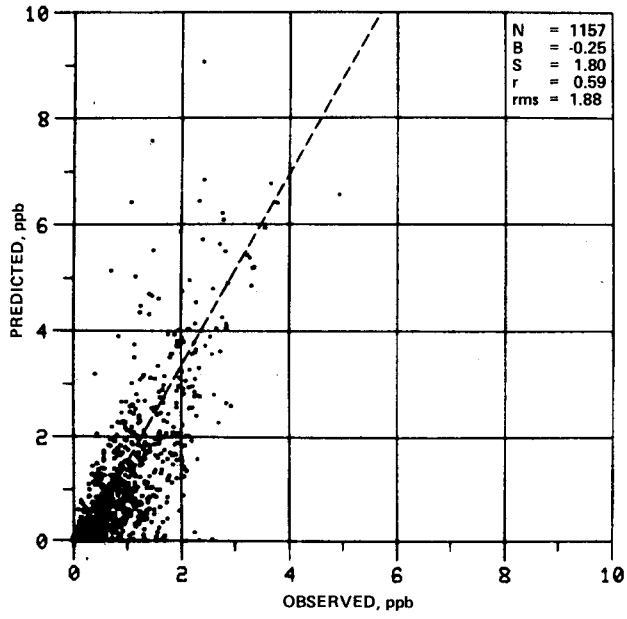

FIG. 19. As in Fig. 15 except wake turbulence and velocity deficit are omitted.

roadway ($u=0.12$ m s^{-1} and $v=2.54$ m s^{-1} at 1.5 m). Figs. 10 and 11 show the eddy diffusion coefficients and winds from similarity theory, while Figs. 12 and 13 show the K_x^w and K_z^w fields from the wake theory. It should be noted that the maximum concentration values in the parallel wind cases are larger than those of crosswind cases. Figs. 14 shows the calculated and observed concentration fields of SF_6 near the roadway, and in this case the agreement is very good. However, as will be shown later, the model tends to overpredict in parallel winds.

The composite results of the 58 half-hour simulations are shown in Figs. 15–19, while Fig. 20 shows a scatter diagram of results from the EPA highway model (Petersen, 1976). Comparison of Figs. 15 and 20 shows that the finite-difference model does a better job of predicting the maximum values observed in the GM experiment. (The number of points in Fig. 20 is less than that shown in Fig. 15 because the Gaussian model does not predict upwind concentrations.) One also notices that the slope of the linear least-squares fit line is much closer to 1 and that the correlation is higher for the finite-difference model than for the EPA Gaussian model. In order to see the effect the wakes have on the results all the cases were run neglecting the wake effect; as can be seen in Fig. 19 the results are very close to those in Fig. 20 for the Gaussian highway model.

In Fig. 16 the correlation between observations and predictions for each instrument location is shown by tower number and height. The indication here is that processes near the road are *not* being treated with complete accuracy.

Fig. 17 is a plot of the correlation between observations and predictions for the observation network for each half-hour period. The correlation is generally very high, and if there is a trend, it is that the correlation increases as time of day increases. In other words, as the stability decreases (more unstable), the correlation increases.

Fig. 18 is a frequency distribution plot of $(O-P)/O$, where O represents prediction. Ideally, the distribution, in this figure would be Gaussian indicating that the errors are random. However, this plot is not Gaussian and Fig. 18 indicates that there is some tendency to overpredict in the model.

The data were divided into two sets to aid in analyzing the tendency of the model to overpredict—the first a cross-wind data set and the second a parallel data set. Scatter diagrams for these two cases are shown in Figs. 21 and 22. Fig. 20, which is the cross-wind case, shows that the model tends to slightly underpredict and Fig. 22 indicates that the model overpredicts for parallel winds.

The one physical process that has not been included is the effect of heat emissions from the automobiles on the atmosphere. When the winds have a cross-road component ($|u|>0.5$ m s^{-1}), it can be shown that the heat input per unit mass is very low and can be ignored. These facts indicate that the underprediction in the cross-wind case is because K_z^w and K_x^w are too large. This overprediction of K_x^w, K_z^w can easily be accounted for in the uncertainty of a_1,a_2,a_3 determined earlier by Eskridge and Hunt (1979). For the parallel wind case it becomes clear that neglecting the heat input of vehicles contributes to an overprediction of concentration. It does not account for all of the over-

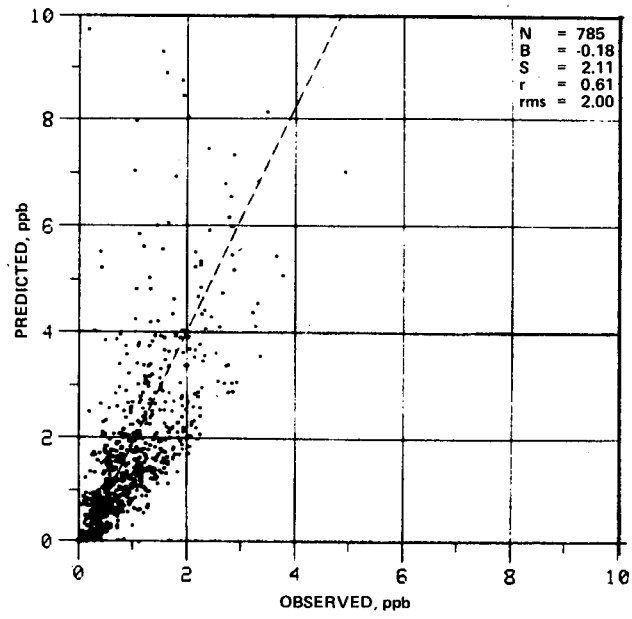

FIG. 20. As in Fig. 15 except for the EPA highway model.

prediction since meander of the wind cannot be accounted for in this type of model.

There are two possible effects that the heat emission can have: first, the heat released adds buoyancy to the air leading to vertical motion; second, the heat released can change the local stability structure near the roadway causing an increase in the vertical diffusion. Rao *et al.* (1979) have found in stable conditions along a New York roadway that the heat flux is downward and that there is no organized convection. It follows that under stable conditions the heat input by the vehicle can significantly change the stability near the road, which is evident in the GM data.

One is tempted to parameterize the temperature increase downwind of the roadway by using dimensional analysis. The most reasonable formulation is

$$\frac{c_p\Delta T}{\Delta H}=F\left(\mathrm{R}_b,\frac{x}{D},\frac{z}{D}\right), \tag{50}$$

where $\Delta H=G(N_v,V_h,\rho,u,v)$, N_v is the number of vehicles, V_h the speed of the vehicles, ρ the density of the air, and u and v the wind components. In the GM experiment the horizontal distance downwind of the road is fixed since there are only two towers; thus by picking one level Eq. (50) becomes

$$\frac{c_p\Delta T}{\Delta H}=F_1(\mathrm{R}_b). \tag{51}$$

The function F_1 could be determined for the unstable case and was best approximated by a linear relationship. However, it was not possible to find a function F_1 which fit the data with any reasonable degree of goodness of fit for the stable conditions.

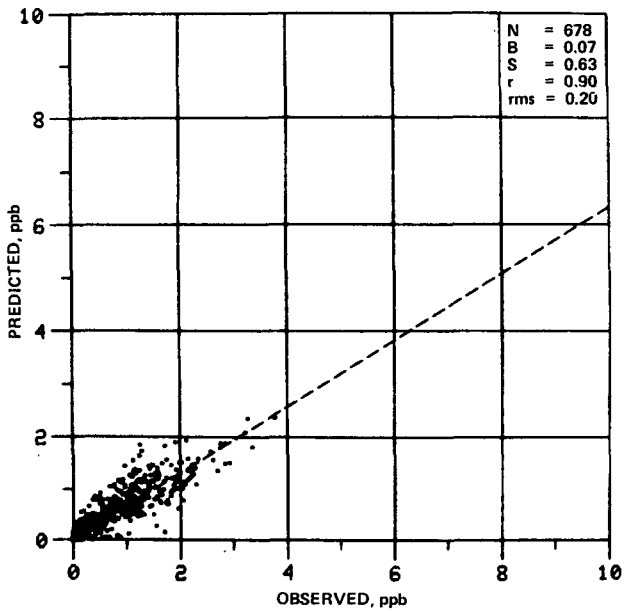

FIG. 21. As in Fig. 15 except for cross winds only.

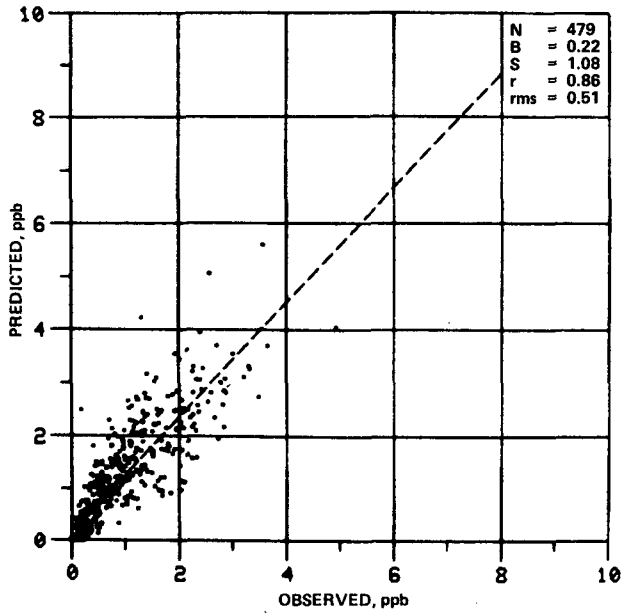

FIG. 22. As in Fig. 15 except for parallel winds only.

The most reasonable explanation for this failure is that under stable conditions the vehicle wakes are transporting heat downward and obscuring any relationship such as (51). Another possibility is that the vehicle wakes are mixing heat upward from the road which will be warmer than the air. However, this effect is probably small for the GM study which took place in the morning hours of September and October.

7. Summary

This study shows that improved treatment of the physics of the atmosphere and vehicle effects can improve the prediction of pollution concentration along a roadway. The model presented here uses the wake theory of Eskridge and Hunt (1979), which is applicable when vehicle speed is much greater than the ambient wind speed.

The process that has not been included in this model is the change in stability near the roadway due to heat release by the vehicles. The failure of a simple parameterization via dimensional analysis using the GM data suggests that another approach is needed.

APPENDIX

Donar Cell Flux-Corrected Transport Algorithm

The following numerical scheme was invented by S. Zalesak of the Naval Research Laboratories and is presented with his permission. The one-dimensional advection scheme presented here is a modification

and generalization of a scheme presented in Book *et al.* (1975).

For the advection equation

$$\frac{\partial \rho}{\partial t}+\frac{\partial u\rho}{\partial x}=0, \tag{A1}$$

the numerical method proceeds as follows:

Define

$$\tilde{\rho}^{n+1}=\frac{M_i+\Delta M_{i-\frac{1}{2}}-\Delta M_{i+\frac{1}{2}}}{x_{i+\frac{1}{2}}-x_{i-\frac{1}{2}}} \tag{A2}$$

$$M_i=\rho_i^n(x_{i+\frac{1}{2}}-x_{i-\frac{1}{2}}) \tag{A3}$$

$$\Delta M_{i+\frac{1}{2}}=\begin{cases}u_{i+\frac{1}{2}}\Delta t\rho_i^+, & u_{i+\frac{1}{2}}>0\\ u_{i+\frac{1}{2}}\Delta t\rho_{i+1}^-, & u_{i+\frac{1}{2}}<0\end{cases} \tag{A4}$$

$$\rho_i^+=\rho_i^n(x_i-x_{i-1})/(x_i^L-x_{i-1}^L) \tag{A5}$$

$$u_{i+\frac{1}{2}}=\frac{u_i+u_{i+1}}{2} \tag{A6}$$

$$x_{i+\frac{1}{2}}=\frac{x_{i+1}+x_i}{2} \tag{A7}$$

$$x_i^L=x_i+u_i\Delta t. \tag{A8}$$

It follows that $\tilde{\rho}_i^{n+1}$ is the normal upstream difference quantity at the time level $n+1$. Next the antidiffusion fluxes $A_{i+\frac{1}{2}}^*$ are calculated, limits are imposed and the fluxes $A_{i+\frac{1}{2}}$ are determined, which are used to anti-diffuse $\tilde{\rho}_i^{n+1}$ to produce ρ_i^{n+1}. We then proceed as follows:

$$A_{i+\frac{1}{2}}^*=(\rho_{i+1}^--\rho_i^+)\frac{|u_{i+\frac{1}{2}}|\Delta t}{2}\left(1.0-\frac{|u_{i+\frac{1}{2}}|\Delta t}{x_{i+1}^L-x_i^L}\right) \tag{A9}$$

$$\Delta_{i+\frac{1}{2}}=\tilde{\rho}_{i+1}^{n+1}-\tilde{\rho}_i^{n+1} \tag{A10}$$

$$S_{i+\frac{1}{2}}=\text{sign}(1.0,A_{i+\frac{1}{2}}^*) \tag{A11}$$

$$A_{i+\frac{1}{2}}=S_{i+\frac{1}{2}}\,\text{Max}[0.0,\,\text{Min}\{S_{i+\frac{1}{2}}\Delta_{i-\frac{1}{2}}(x_{i+\frac{1}{2}}-x_{i-\frac{1}{2}}),\ |A_{i+\frac{1}{2}}^*|,\ S_{i+\frac{1}{2}}\Delta_{i+\frac{3}{2}}(x_{i+\frac{3}{2}}-x_{i+\frac{1}{2}})\}] \tag{A12}$$

$$\rho_i^{n+1}=\tilde{\rho}_i^{n+1}+\frac{A_{i-\frac{1}{2}}-A_{i+\frac{1}{2}}}{x_{i+\frac{1}{2}}-x_{i-\frac{1}{2}}}. \tag{A13}$$

It should be noted that this technique allows unequal grid sizes and is very useful in highway modeling where high resolution is needed at the roadway and the resolution can be decreased rapidly away from the roadway.

REFERENCES

Benoir, R., 1977: On the integral of the surface layer profile-gradient functions. *J. Appl. Meteor.*, **16**, 859–860.

Binkowski, F. S., 1979: A simple semiempirical theory for turbulence in the atmospheric surface layer. *Atmos. Environ.* (in press).

Book, D. L., J. P. Boris and K. Han, 1975: Flux-corrected transport II. Generalization of the method. *J. Comput. Phys.*, **18**, 248–283.

Boris, J. P., and D. L. Book, 1973: Flux-corrected transport. I. SHASTA A fluid transport algorithm that works. *J. Comput. Phys.*, **11**, 38–69.

Busch, N. E., 1973: On the mechanics of atmospheric turbulence. *Workshop on Micrometeorology*, D. A. Haugen, Ed., Amer. Meteor. Soc., 1–61.

Cadle, S. H., D. P. Chock, J. M. Heuss and P. R. Monson, 1976: Results of the General Motors sulfate dispersion experiments. General Motors Res. Publ. GMR-2107, Warren, MI, 140 pp.

Chock, D. P., 1977: General Motors sulfate dispersion experiment—An overview of the wind, temperature, and concentration fields. *Atmos. Environ.*, **11**, 553–559.

Danard, M. B., 1972: Numerical modelling of carbon monoxide concentrations near highways. *J. Appl. Meteor.*, **11**, 947–957.

Dyer, A. J., 1974: A review of flux-profile relationships. *Bound.-Layer Meteor.*, **7**, 363–372.

Egan, B. A., A. Epstein and M. Keefe, 1973: Development of procedures to simulate motor vehicle pollution levels. Final Report, D.C. Department of Highways and Traffic [NTIS PB-233-938].

Eskridge, R. E., and K. L. Demerjian, 1977: Evaluation of numerical schemes for solving a conservation of species equation with chemical terms. *Atmos. Environ.*, **11**, 1029–1035.

——, and J. C. R. Hunt, 1979: Highway modeling part I—Prediction of velocity and turbulence fields in the wake of vehicles. *J. Appl. Meteor*, **18**, 387–400.

Hanna, S. R., 1968: A method of estimating the vertical eddy transport in the planetary boundary layer using the characteristics of the verticle velocity spectrum. *J. Atmos. Sci.*, **25**, 1026–1033.

Hinze, J. O., 1975: *Turbulence.* McGraw-Hill, 790 pp.

Kaimal, J. C., 1973: Turbulence spectra, length scales and structure parameters in the stable surface layer. *Bound.-Layer Meteor.*, **4**, 289–309.

Kirsch, J. W., and B. F. Mason, 1974: EXPLOR-examination of pollution levels of roadways. Final Report, California Air Resources Board [NTIS PB-236-713].

Marchuk, G. I., 1975: *Methods of Numerical Mathematics.* Springer Verlag, 316 pp. (Translated by Jiri Ruzicka.)

Nickerson, E. C., and V. E. Smiley, 1975: Surface layer and energy budget parameterization for mesoscale models. *J. Appl. Meteor.*, **14**, 297–300.

Petersen, W. B., 1976: Comparison of dispersion model estimates with measured sulfate concentrations. The General Motors/Environmental Protection Agency sulfate dispersion experiment—selected EPA research papers, Rep. EPA 600/3-76-035, Research Triangle Park, NC, 149 pp.

Ragland, K. W., and J. J. Peirce, 1973: Air pollution due to highway traffic. Working Pap. 13, University of Wisconsin [NTIS PB-228-691].

Rao, S. T., L. Sedefian and U. H. Czapski, 1979: Characteristics of turbulence and dispersion of pollutants near major highways. *J. Appl. Meteor.*, **18**, 283–293.

Wamser, C., and H. Müller, 1977: On the spectral scale of wind fluctuations within and above the surface layer. *Quart. J. Roy. Meteor. Soc.*, **103**, 721–730.